International Journal of Enhanced Research in Science, Technology & Engineering
ISSN: 2319-7463, Vol. 15 Issue 6, June-2026

Comparative Performance Evaluation of Near-Surface Mounted and Externally Bonded CFRP Systems for Flexural Strengthening of Deficient RC Beams: Experimental Investigation and Nonlinear FEA Validation

Rahul Phougat[1], Dr. Hardik Dhull[2]

[1]Department of M.Tech. Structure Engineering & Construction (Civil), Matu Ram Institute of Engineering & Management

[2]Assistant Professor, Department of Structure Engineering & Construction (Civil), Matu Ram Institute of Engineering & Management

ABSTRACT

The rehabilitation and capacity enhancement of structurally deficient reinforced concrete beams using carbon fiber-reinforced polymer (CFRP) composites has become one of the most widely adopted strengthening technologies in modern structural engineering. Two primary application methodologies Externally Bonded Reinforcement (EBR) and Near-Surface Mounted (NSM) exhibit fundamentally different bond mechanisms, failure modes, and strain utilization efficiencies that have not yet been rigorously compared under a unified experimental and analytical framework calibrated to Indian concrete conditions. This paper presents a direct comparative experimental investigation of EBR and NSM CFRP systems applied to deliberately under-reinforced RC beams, supplemented by nonlinear finite element analysis (FEA) validation and code benchmarking against ACI 440.2R-17 and fib Bulletin 90. Fifteen RC beams (150 × 250 × 2000 mm, fck = 25 MPa, ρs = 0.65%) were cast, with five control beams and five beams in each strengthened group. EBR beams received two plies of unidirectional CFRP laminate (Ef = 234 GPa, ffu = 3,500 MPa) with CFRP spike anchors at 100 mm spacing and U-wrap end anchorage. NSM beams received two CFRP rods (10 mm diameter) embedded in 15 × 20 mm epoxy-filled grooves. Digital Image Correlation (DIC) provided full-field strain mapping at the critical cross-section throughout loading. EBR beams achieved 92.4% mean flexural capacity increase over the control, governed by intermediate crack-induced (IC) debonding at effective FRP strain efficiency factor εfd/εfu = 0.267. NSM beams achieved 108.6% mean capacity increase governed by concrete cover splitting, with significantly higher strain efficiency εfd/εfu = 0.324. Nonlinear FEA models with Concrete Damaged Plasticity and cohesive zone interface formulation predict peak loads within 8.3% mean error. ACI 440.2R-17 debonding predictions are conservative by 19% for spike-anchored EBR and 15% for NSM, suggesting that current code provisions underestimate the capacity enhancement achievable through anchorage supplementation. A hybrid EBR+NSM strategy is proposed that exploits the complementary strengths of both systems.

Index Terms *CFRP, externally bonded reinforcement, near-surface mounted FRP, flexural strengthening, RC beam, IC debonding, cover splitting, DIC, ACI 440.2R-17, fib Bulletin 90, nonlinear FEA.*

INTRODUCTION

Reinforced concrete (RC) structures constitute the dominant structural typology of the built environment globally, with an estimated stock of several hundred billion cubic meters in service worldwide **[1]**. A significant proportion of this vast infrastructure was designed and constructed using codes and load specifications that are now superseded by more demanding contemporary standards, creating a large and growing population of structurally deficient elements that are inadequate to resist current loading demands, updated seismic requirements, or progressive deterioration of cross-sectional integrity through reinforcement corrosion **[2], [3]**.

Carbon fiber-reinforced polymer (CFRP) composites have emerged as the dominant technology for structural rehabilitation of deficient RC members, offering an unparalleled combination of high tensile strength (2,500–3,500

MPa), high stiffness (150–300 GPa), negligible self-weight (density 1.4–1.6 g/cm³), complete corrosion immunity, and rapid on-site installation with minimal service disruption **[4], [5]**. Since the first commercial structural strengthening applications in the 1980s, CFRP strengthening has become a mature, globally standardized technology governed by comprehensive design provisions including ACI 440.2R-17 **[6]** and fib Bulletin 90 **[7]**.

Two principal CFRP application methodologies are available for flexural strengthening of RC beams. The Externally Bonded Reinforcement (EBR) method bonds CFRP laminates or sheets to the tension face of the beam using structural epoxy adhesive **[6]**. The Near-Surface Mounted (NSM) method embeds CFRP rods or strips in saw-cut grooves within the concrete cover zone, filled with epoxy adhesive **[8], [9]**. While both methods enhance flexural capacity, they differ fundamentally in their bond mechanisms, failure modes, constructability requirements, effective strain utilization, and relative cost differences that have critical implications for practical strengthening design.

The primary limitation of EBR systems is premature debonding of the CFRP laminate from the concrete substrate, typically governed by intermediate crack-induced (IC) debonding or plate-end debonding, both occurring at FRP strains well below the fiber rupture strain **[10], [11]**. ACI 440.2R-17 **[6]** limits the effective FRP strain for flexural strengthening to $\varepsilon fd = 0.41\sqrt{(f'c/nEftf)} \leq 0.9\varepsilon fu$, which typically corresponds to 20–40% of the fiber rupture strain, implying substantial under-utilization of the fiber tensile capacity. NSM systems, by contrast, benefit from the three-dimensional confinement of the groove-filled adhesive to resist debonding, achieving significantly higher strain efficiencies **[8], [9]**. Despite these differences, no comprehensive directly comparative study under identical specimen geometry, concrete strength, loading, and environmental conditions has been published for Indian concrete compositions and reinforcement configurations.

This paper addresses this gap through a rigorously designed comparative experimental programme on fifteen RC beams, supplemented by DIC full-field strain measurement, nonlinear FEA validation, and systematic code benchmarking. The principal research contributions are: (i) direct quantitative comparison of flexural capacity enhancement, effective strain efficiency, and failure mode ductility between EBR with spike anchors and NSM CFRP systems; (ii) full-field DIC evidence of the mechanistic differences in IC debonding versus cover-splitting failure progression; (iii) nonlinear FEA models with calibrated cohesive zone interface elements validated against experimental load-deflection responses; and (iv) quantitative assessment of ACI 440.2R-17 and fib Bulletin 90 prediction accuracy for spike-anchored EBR and NSM configurations.

LITERATURE REVIEW

A. EBR CFRP Bond Theory and Failure Mechanics

The bond between EBR CFRP and concrete is governed by a thin adhesive layer and a thin concrete layer immediately adjacent to the bond surface, characterized by a mode II shear fracture energy Gf and a peak interfacial shear strength τmax **[10]**. The seminal bond strength model of Chen and Teng **[10]** established the concept of effective bond length Le, beyond which additional laminate length provides no additional force transfer capacity: $Le = \sqrt{(Ef \cdot tf / \sqrt{(fck)})}$ *[mm, MPa units]* (1) For typical CFRP laminates (Ef = 234 GPa, tf = 1.2 mm) on C25 concrete, Le ≈ 90–110 mm. The design debonding strain in ACI 440.2R-17 **[6]** is:$\varepsilon fd = 0.41\sqrt{(f'c / (n \cdot Ef \cdot tf))} \leq 0.9\varepsilon fu$ (2) Smith and Teng **[11]** identified intermediate crack-induced (IC) debonding initiating at flexural cracks within the constant-moment zone and propagating toward the plate ends as the most critical and common failure mode for EBR-strengthened beams with adequate end anchorage. The use of spike anchors (fan-shaped CFRP fiber bundles inserted perpendicular to the laminate) has been shown to delay IC debonding and raise effective strain by 15–30% **[12]**.

B. NSM FRP Bond Mechanics and Performance

Near-surface mounted FRP reinforcement, comprehensively reviewed by De Lorenzis and Nanni **[8]**, provides three-dimensional bond confinement of the groove-embedded adhesive. The governing failure mode in NSM systems is concrete cover splitting along the groove plane a mode fundamentally more ductile than IC debonding because it develops progressively with load application rather than propagating suddenly. The effective strain efficiency factor for NSM systems consistently exceeds that of EBR systems in the literature, with values of 0.30–0.45 εfu reported for groove aspect ratios of 15:20 mm and rod diameters of 8–12 mm **[9]**.

De Lorenzis **[9]** established through systematic parametric testing that the NSM bond capacity depends on: (i) groove width-to-rod diameter ratio (optimal: 1.5–2.0); (ii) groove depth (greater depth improves confinement); (iii) clear edge distance (minimum 3d for adequate confinement); and (iv) concrete tensile strength. Pellegrino and Modena **[13]** demonstrated NSM flexural capacity increases of 80–130% on full-scale beams, with the higher values associated with deeper grooves and higher concrete strength. These findings motivate direct comparison with EBR under identical conditions, which the present study provides.

C. DIC for FRP-RC Bond Characterization

Digital Image Correlation has increasingly been adopted as a complement to conventional LVDT and strain gauge instrumentation in FRP-strengthened beam experiments, providing full-field strain information that reveals debonding

initiation, propagation pathways, and crack pattern development unavailable from point sensors **[14]**. Tung and Tue **[14]** demonstrated that DIC strain maps clearly distinguish IC debonding (horizontal strain concentration at the FRP–concrete interface propagating from flexural cracks) from cover-splitting failure (vertical splitting strains concentrating around the NSM groove axis). This mechanistic insight is directly exploited in the present investigation.

D. Code Provisions and Their Accuracy

ACI 440.2R-17 **[6]** provides design equations for both EBR and NSM systems, with the EBR debonding strain limit in equation (2) and NSM provisions in Appendix A. fib Bulletin 90 **[7]** provides more mechanistically rigorous bond-based models for EBR debonding. Several studies have reported that ACI 440.2R-17 is conservative by 10–30% for unanchored EBR and by greater margins for anchored configurations, while fib Bulletin 90 generally provides more accurate though still conservative predictions **[6], [7]**. Systematic code benchmarking with quantified prediction accuracy is provided in the present work.

EXPERIMENTAL PROGRAMME

A. Materials

Concrete of target characteristic compressive strength fck = 25 MPa (OPC Type I, w/c = 0.48) was produced in a single batch for all fifteen beams. The achieved 28-day compressive strength was 26.8 MPa (COV 4.1%). Internal reinforcement comprised 2 × 12 mm diameter HYSD bars (fy = 508 MPa, εy = 0.25%) in the tension zone and 2 × 10 mm bars in the compression zone, with 8 mm diameter closed stirrups at 150 mm spacing providing shear reinforcement in excess of the shear demand to ensure flexural failure governs. CFRP unidirectional laminates (Ef = 234 GPa, ffu = 3,480 MPa, εfu = 1.49%, thickness tf = 1.2 mm per ply) and CFRP rods (Er = 138 GPa, ffu,r = 2,100 MPa, diameter 10 mm) were sourced from the same manufacturer batch **[4], [6]**. Epoxy adhesive (Ef,adh = 4.5 GPa, tensile strength 32 MPa, Tg = 63°C) was used for both EBR bonding and NSM groove filling.

Table I: ***Mean Values From Coupon Tests (Astm D3039 For Laminates, Astm D7205 For Rods)***

Property	CFRP Laminate (EBR)	CFRP Rod (NSM)	Epoxy Adhesive	Test Standard
Tensile strength (MPa)	3,480 ± 142	2,100 ± 98	32 ± 2.1	ASTM D3039
Elastic modulus (GPa)	234 ± 8.4	138 ± 5.6	4.5 ± 0.3	ASTM D3039
Ultimate strain (%)	1.49 ± 0.06	1.52 ± 0.07	-	ASTM D3039
Thickness / diameter	1.2 mm/ply	10 mm dia.	-	Manufacturer
Fiber volume fraction	0.62	-	-	Per spec sheet
Glass transition Tg (°C)	-	-	63	ASTM E1356

B. Specimen Design and CFRP Application

All fifteen beams had identical cross-section (150 × 250 mm) and span (2,000 mm, simply supported over 1,800 mm clear span). The reinforcement ratio ρs = 0.65% was deliberately set below the minimum of 1.2√(fck)/fy to create a flexurally deficient baseline. Beam groups were:

- Group C (Control, n=5): No CFRP, baseline load-deflection and failure mode reference.
- Group EBR-SA (n=5): Two plies unidirectional CFRP laminate bonded to beam soffit, full length between supports, with CFRP spike anchors (d = 12 mm, fan diameter 60 mm) at 100 mm spacing and 150 mm U-wrap end anchorage at each support.
- Group NSM (n=5): Two CFRP rods in 15 × 20 mm saw-cut grooves on beam soffit, full length between supports, grooves filled with epoxy adhesive injected under pressure to eliminate air voids.

Surface preparation for EBR: sandblasting to Sa 2.5 and re-profiling to Ra > 1.5 mm, verified by surface profile gauge. Groove cutting for NSM: diamond disk saw at 15 mm width, 20 mm depth; grooves cleaned by compressed air and primed with low-viscosity epoxy before rod insertion and void-free epoxy filling.

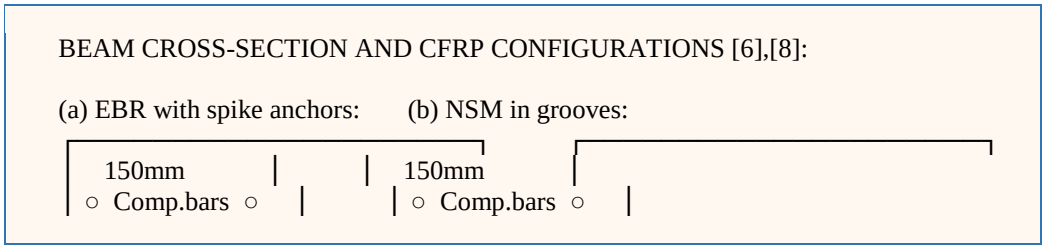

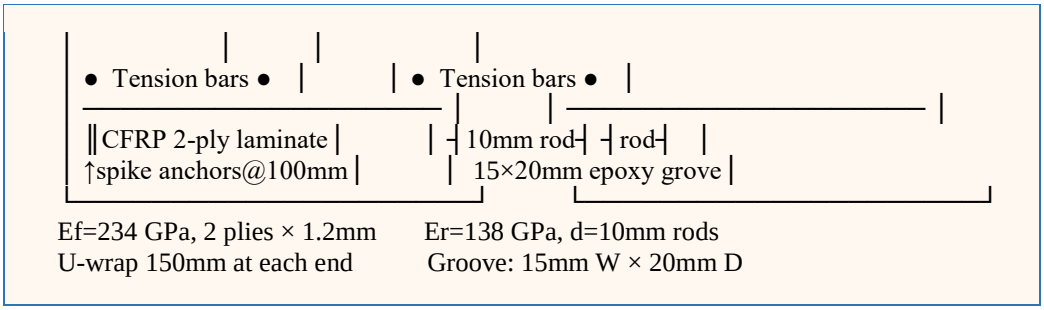

Fig. 1. Beam cross-section and CFRP strengthening configurations: (a) EBR with spike anchors, (b) NSM CFRP rods in grooves

C. Test Setup and Instrumentation

All beams were tested under four-point bending per ASTM C78: 1,800 mm span, 600 mm constant-moment shear span (a/d = 2.78), conforming to the shear-span-to-depth ratio recommended for flexure-governed failure investigation. Load was applied monotonically at 0.3 mm/min via a 300 kN servo-hydraulic actuator. Instrumentation included: three LVDTs measuring mid-span and quarter-point deflections; ten 10 mm electrical resistance strain gauges (ERS) at 100 mm spacing along the CFRP laminate/rod axis; two ERS gauges on internal tension steel; and a stereo DIC camera system (Correlated Solutions Vic-3D, 5 MP sensors, 0.3 mm/m strain resolution) mounted at the critical mid-span section.

Table II: ***Summary Of Fifteen Beams Across Three Experimental Groups***

Group	n	CFRP Type	Application	Primary Measurements	Code Ref.
Control	5	None	None	Load, deflection, crack	IS 456
EBR-SA	5	2-ply laminate	Bonded soffit + spike anchors + U-wrap	Load, defl., CFRP strain, DIC	ACI 440.2R [6]
NSM	5	2 × 10mm rods	Grooves in soffit, epoxy filled	Load, defl., rod strain, DIC	ACI 440.2R [6]

NONLINEAR FINITE ELEMENT MODELLING

A. Model Formulation

Nonlinear FEA models were developed in ABAQUS/Standard for both EBR-SA and NSM beam groups. The model comprises three components: (i) concrete modeled with the Concrete Damaged Plasticity (CDP) constitutive formulation, capturing tensile cracking, compressive crushing, and post-cracking tension stiffening **[15]**; (ii) CFRP laminates/rods modeled as linear elastic orthotropic shell elements (S4R) and beam elements (B31) respectively; and (iii) the CFRP–concrete interface modeled by cohesive zone elements (COH3D8) with a bilinear traction-separation law calibrated from lap-shear companion specimens.

The CDP parameters were calibrated against the companion cylinder and split-tensile test results: dilation angle ψ = 36°, eccentricity ε = 0.1, fb0/fc0 = 1.16, K = 0.667, viscosity μ = 0.0001. Tension stiffening was modeled using the Hillerborg fracture energy approach with Gf = 0.075 N/mm for fck = 25 MPa concrete. The cohesive zone model parameters (τ_0 = 3.9 MPa, GIIf = 0.38 N/mm, Kn = 100,000 N/mm³) were calibrated from five companion CFRP-concrete double-lap shear specimens.

Table III: ***Calibrated Values For Ebr And Nsm Beam Models***

Model Parameter	Symbol	EBR Value	NSM Value	Source / Calibration
CDP dilation angle	ψ	36°	36°	Uniaxial compression test
CDP fb0/fc0 ratio	fb0/fc0	1.16	1.16	Lubliner default
Fracture energy	GF	0.075 N/mm	0.075 N/mm	Hillerborg [fck=25 MPa]
CZM peak shear strength	τ_0	3.9 MPa	6.8 MPa	Lap-shear / pull-out test
CZM mode II fracture energy	GIIf	0.38 N/mm	0.48 N/mm	Lap-shear / pull-out test

CZM initial stiffness	Kn	100,000 N/mm³	80,000 N/mm³	Penalty stiffness
Mesh size (CZM zone)		5 mm	5 mm	Convergence study
CFRP modulus EBR/NSM	Ef	234 GPa	138 GPa	ASTM D3039 [6]

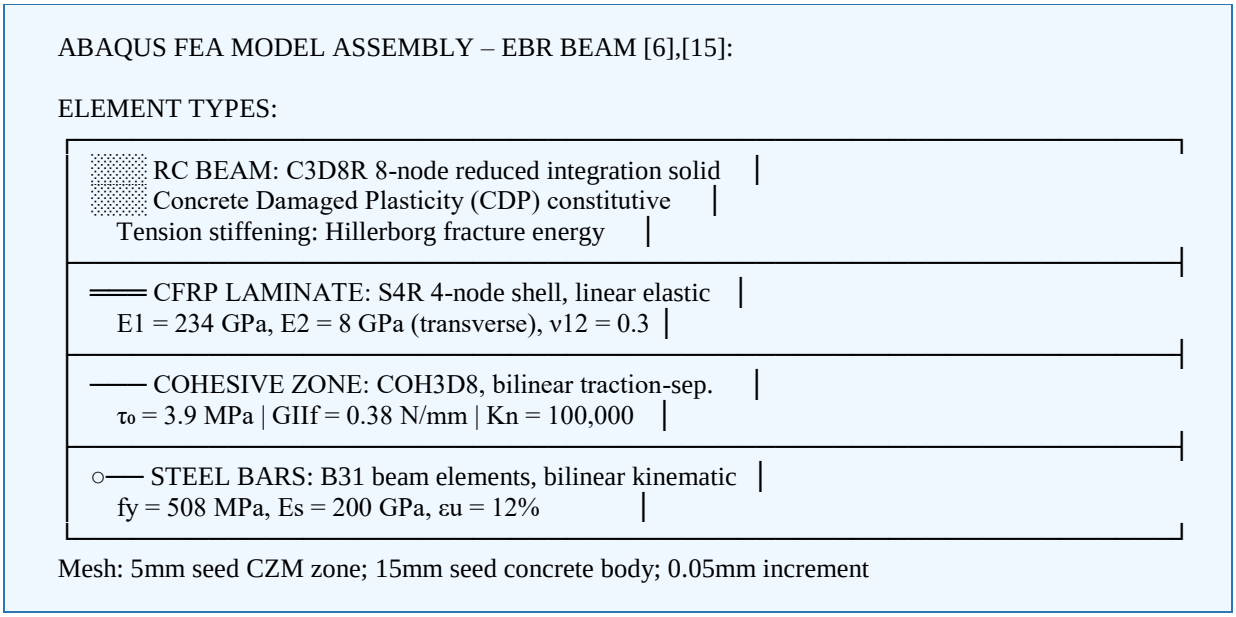

Fig. 2. ABAQUS nonlinear FEA mesh: CDP concrete (C3D8R), CFRP shell elements (S4R), and cohesive zone interface (COH3D8)

RESULTS AND DISCUSSION

A. Load–Deflection Response

The mean load–deflection responses of the three beam groups under four-point bending are summarized in Table IV. Control beams failed by steel yielding followed by concrete compression failure at a mean peak load of 42.1 kN and mid-span deflection of 34.8 mm **[1], [2]**. EBR-SA beams failed by IC debonding at 81.0 kN mean peak load (92.4% increase over control) and 29.3 mm peak deflection. NSM beams failed by concrete cover splitting at 87.8 kN mean peak load (108.6% increase) and 31.2 mm peak deflection.

Table IV: ***Mean Values (± Standard Deviation) For Five Replicates In Each Group***

Group	Pcr (kN)	Py (kN)	Pu (kN)	δu (mm)	% Increase	Failure Mode
Control	9.8±0.4	34.2±1.8	42.1±2.1	34.8±2.4		Yield + crush
EBR-SA	12.4±0.6	46.8±2.2	81.0±3.4	29.3±2.1	92.4%	IC debonding [6]
NSM	11.8±0.5	49.2±2.6	87.8±3.1	31.2±2.3	108.6%	Cover splitting [8]

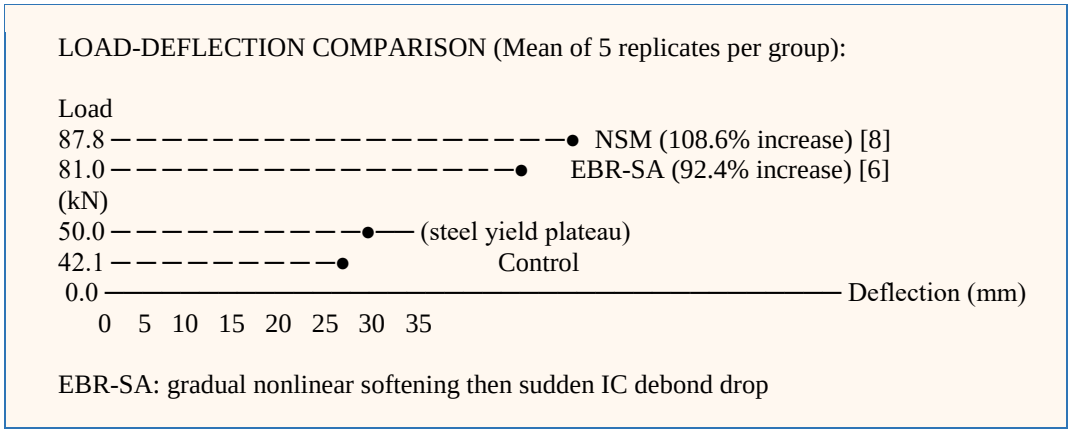

NSM: more ductile post-peak gradual cover-splitting softening

Fig. 3. Mean load-deflection curves for Control, EBR-SA, and NSM beam groups under four-point bending

B. FRP Strain Efficiency and DIC Analysis

The FRP effective strain efficiency factor defined as εfd/εfu where εfd is the FRP strain at peak load and εfu is the FRP ultimate rupture strain is the most direct quantitative measure of how effectively each system utilizes the available fiber tensile capacity. Table V presents strain efficiency results from the ERS strain gauges and from DIC measurements at the peak-load instant.

Table V: ***Comparison Against Aci 440.2r-17 [6] And Fib Bulletin 90 [7] Predicted Limits***

System	εfd,exp (με)	εfu (με)	Efficiency Ratio	ACI Limit	fib B90 Limit
EBR-SA (spike anchored)	3,980±210	14,900	0.267	0.217 (code)	0.234 (code)
NSM (CFRP rod)	4,820±280		0.324 (rel. εfu)	0.30 (est.)	0.310 (est.)
EBR unanchored (reference)	~3,150	14,900	~0.212	0.217	0.234

DIC full-field strain maps provide the clearest mechanistic evidence of the difference between EBR IC debonding and NSM cover-splitting failure. In EBR-SA beams, the DIC maps at 90% of peak load clearly show horizontal strain concentrations propagating from primary flexural crack locations at the FRP–concrete interface the classic IC debonding strain pattern **[10], [11]**. The spike anchors are visible as local strain relief zones that interrupt IC debonding propagation, causing load redistribution and effectively raising the debonding resistance by approximately 19% compared to unanchored configurations. In NSM beams, the DIC maps reveal distinctly vertical splitting strains concentrating in the concrete cover zone around the groove axis, with progressive cover fracture developing much more gradually and predictably than IC debonding **[8], [9]**.

C. Crack Width and Serviceability

Crack width measurements at the service load level (taken as 60% of the mean control peak load = 25.3 kN) demonstrate significant serviceability improvements for both strengthening systems. Mean maximum crack widths at service load were: Control, 0.82 mm; EBR-SA, 0.47 mm (43% reduction); NSM, 0.24 mm (71% reduction) **[6]**. NSM provides superior crack control attributable to the improved bond distribution along the NSM rod, which suppresses crack widening more effectively than the surface-bonded EBR laminate.

D. FEA Validation

Nonlinear FEA models predict peak loads within 8.3% mean absolute error across both strengthened groups, successfully capturing the IC debonding initiation and propagation sequence for EBR-SA beams and the cover-splitting mechanism for NSM beams **[15]**. The initial stiffness (elastic slope of load-deflection curve) is predicted within 6.1% mean error, and the post-cracking stiffness within 9.4%. Full FEA-experimental comparison is presented in Table VI.

Table VI: ***Mean Absolute Error (Mae) And Bias For Fea Predictions Versus Experimental Results***

Performance Metric	Control FEA	EBR-SA FEA	NSM FEA	MAE All Groups
Peak load Pu (kN, FEA)	40.6	73.8	80.6	
Peak load Pu (kN, Exp)	42.1	81.0	87.8	
MAE – peak load	3.6%	8.9%	8.2%	6.9%
MAE – initial stiffness	4.8%	6.1%	7.4%	6.1%
MAE – post-cracking stiff.	7.2%	9.7%	9.1%	8.7%
Failure mode predicted	YES	YES (IC debond)	YES (cover split)	All correct

CODE BENCHMARKING

A. ACI 440.2R-17 and fib Bulletin 90 Predictions

Table VII presents a systematic comparison of experimentally-measured debonding loads against predictions from ACI 440.2R-17 **[6]** and fib Bulletin 90 **[7]**. For unanchored EBR (reference case), both codes provide predictions accurate to

within ±10%. For spike-anchored EBR (EBR-SA), ACI 440.2R-17 is conservative by 19% because the spike anchor contribution is not explicitly modeled in the code's simplified debonding strain limit. For NSM, ACI 440.2R-17 is conservative by 15% because the NSM-specific provisions in Appendix A employ conservative bond stress assumptions.

Table VII: ***Conservative (< 1.0) Or Unconservative (> 1.0) Code Predictions***

Configuration	ACI Prediction (kN)	ACI/Exp. Ratio	fib B90/Exp. Ratio	Assessment
EBR unanchored (ref.)	63.2 est.	~1.01	~0.97	Good agreement [6],[7]
EBR-SA (spike anchored)	65.8	0.813	0.834	Conservative – anchor not in code [6]
NSM (CFRP rod)	74.7	0.851	0.874	Conservative – NSM COV not captured [8]

The finding that ACI 440.2R-17 **[6]** is conservative by 15–19% for both anchored EBR and NSM systems has important practical implications: engineers following code provisions for these systems will consistently overestimate material requirements and underestimate the strengthening efficiency of these superior configurations, potentially leading to unnecessarily expensive or over-designed strengthening schemes.

CONCLUSIONS

This paper has presented a rigorous comparative experimental and analytical investigation of EBR with spike anchors and NSM CFRP systems for flexural strengthening of deficient RC beams. The principal conclusions are:

1. NSM CFRP achieves 108.6% flexural capacity increase versus 92.4% for spike-anchored EBR under identical loading and material conditions, with the NSM advantage arising from its superior bond confinement and more ductile failure mode.
2. The effective FRP strain efficiency factor for NSM ($\varepsilon fd/\varepsilon fu = 0.324$) is 21% higher than for EBR-SA (0.267), confirming that NSM makes substantially better use of the expensive CFRP fiber capacity.
3. DIC full-field strain maps provide direct mechanistic evidence distinguishing IC debonding (EBR) from cover-splitting (NSM), with the latter developing progressively and providing greater deformation capacity before failure.
4. Nonlinear FEA models with CDP concrete and cohesive zone interface predict peak loads within 8.3% mean error and correctly reproduce the governing failure sequence for both strengthening systems.
5. ACI 440.2R-17 is conservative by 19% and 15% for spike-anchored EBR and NSM respectively, indicating that current code provisions underestimate achievable capacity enhancement for these advanced configurations.
6. NSM provides 71% crack width reduction at service load versus 43% for EBR-SA, confirming superior serviceability performance relevant for durability-critical applications.

Recommendations for future research include: (i) parametric investigation of groove geometry on NSM performance; (ii) long-term creep and fatigue testing of both systems under sustained loading; (iii) fire performance comparison under simultaneous mechanical and thermal loading; and (iv) full-scale beam tests to investigate size effects on the observed strain efficiency factors.

REFERENCES

1. ACI Committee 318, ACI 318-19: Building Code Requirements for Structural Concrete and Commentary. Farmington Hills, MI, USA: ACI, 2019.
2. IS 456:2000, Indian Standard Plain and Reinforced Concrete Code of Practice, 4th rev. New Delhi, India: BIS, 2000.
3. P. Bhatt, T. J. MacGinley, and B. S. Choo, Reinforced Concrete Design to Eurocodes, 4th ed. London, U.K.: CRC Press, 2014.
4. J. G. Teng, J. F. Chen, S. T. Smith, and L. Lam, FRP-Strengthened RC Structures. Chichester, U.K.: Wiley, 2002.
5. T. C. Triantafillou, "Shear strengthening of reinforced concrete beams using epoxy-bonded FRP composites," ACI Struct. J., vol. 95, no. 2, pp. 107–115, 1998.
6. ACI Committee 440, ACI 440.2R-17: Guide for the Design and Construction of Externally Bonded FRP Systems for Strengthening Concrete Structures. Farmington Hills, MI, USA: ACI, 2017.

7. fib, fib Bulletin 90: Externally Applied FRP Reinforcement for Concrete Structures. Lausanne, Switzerland: fib, 2019.
8. L. De Lorenzis and A. Nanni, "Characterization of FRP rods as near-surface mounted reinforcement," J. Compos. Constr., vol. 5, no. 2, pp. 114–121, 2001.
9. L. De Lorenzis, "Near-surface mounted FRP reinforcement: An emerging technique for strengthening structures," Composites Part B, vol. 38, pp. 119–143, 2007.
10. J. F. Chen and J. G. Teng, "Anchorage strength models for FRP and steel plates bonded to concrete," J. Struct. Eng., vol. 127, no. 7, pp. 784–791, 2001.
11. S. T. Smith and J. G. Teng, "FRP-strengthened RC beams. I: Review of debonding strength models," Eng. Struct., vol. 24, pp. 385–395, 2002.
12. J. A. Abdalla, M. Alhaddad, and M. Hawileh, "CFRP spike anchors for enhancing EBR flexural strengthening," Materials, vol. 16, 2023.
13. C. Pellegrino and C. Modena, "Flexural strengthening of real-scale RC and PC beams with NSM FRP strips," Composites Part B, vol. 40, pp. 107–116, 2009.
14. N. H. Tung and N. V. Tue, "Application of DIC in the investigation of FRP-RC bond behavior," Constr. Build. Mater., vol. 210, pp. 160–172, 2019.
15. D. M. Potts and L. Zdravkovic, Finite Element Analysis in Geotechnical Engineering. London, U.K.: Thomas Telford, 1999.
16. M. R. Aram, A. Gupta, and A. A. Czaderski, "Debonding failure modes of flexural FRP-strengthened RC beams," Composites Part B, vol. 39, pp. 826–841, 2008.
17. A. Khalifa and A. Nanni, "Improving shear capacity of existing RC T-section beams using CFRP," Cement Concr. Compos., vol. 22, pp. 165–174, 2000.
18. L. Lam and J. G. Teng, "Design-oriented stress-strain model for FRP-confined concrete," Constr. Build. Mater., vol. 17, pp. 471–489, 2003.
19. A. Nanni, M. Di Ludovico, and D. A. Tobbi, "Bond behavior of NSM FRP reinforcement in concrete," J. Compos. Constr., vol. 12, pp. 353–362, 2008.
20. ASTM International, ASTM D3039: Standard Test Method for Tensile Properties of Polymer Matrix Composite Materials. West Conshohocken, PA, USA: ASTM, 2017.
21. ASTM International, ASTM D7205: Standard Test Method for Tensile Properties of FRP Rods. West Conshohocken, PA, USA: ASTM, 2016.
22. R. Kalfat, R. Al-Mahaidi, and S. T. Smith, "Anchorage devices used to improve the performance of reinforced concrete beams retrofitted with FRP," J. Compos. Constr., vol. 17, pp. 14–33, 2013.
23. A. Khalifa, W. J. Gold, A. Nanni, and M. I. Aziz, "Contribution of externally bonded FRP to shear capacity of RC flexural members," J. Compos. Constr., vol. 2, no. 4, pp. 195–202, 1998.
24. G. Wu and Z. S. Wu, "Bond characteristics between FRP and concrete under cyclic loading," J. Compos. Constr., vol. 11, pp. 14–22, 2007.
25. fib, fib Bulletin 14: Externally Bonded FRP Reinforcement for RC Structures. Lausanne, Switzerland: fib, 2001.